Int. J. Multiphase Flow Vol. 18, No. 4, pp. 559–576, 1992
Printed in Great Britain.

0301-9322/92 $5.00 + 0.00

A SIMULATION OF PARTICLE DISPERSION IN A TURBULENT JET

D. HANSELL, I. M. KENNEDY and W. KOLLMANN
Department of Mechanical, Aeronautical and Materials Engineering, University of California, Davis, CA 95616, U.S.A.

(Received 12 February 1991; in revised form 28 October 1991)

Abstract—A vortex dynamics calculation of a turbulent jet has been used to study the behavior of discrete particles in an unsteady shear flow. Both axisymmetic and three-dimensional calculations have been performed. It was found that the three-dimensional code did not show significantly different behavior in terms of azimuthal particle disperion from the axisymmetric code under the thin vortex assumption. The full equation for particle dynamics was integrated through the flow field and the results were compared to a calculation which used only the drag force. It was found that the dispersion of droplets was underestimated typically by 25% by the simple approximation, with the greatest errors incurred for large droplets under high-pressure combustor conditions.

Key Words: particle dispersion, vortex dynamics, turbulent shear flow

1. INTRODUCTION

Many devices, including liquid-fueled rocket engines, afterburners, gas turbine combustors, industrial furnaces and diesel engines, utilize heterogeneous or two-phase combustion. Generally, two-phase combustion involves a liquid hydrocarbon fuel which is injected into a hot, high-pressure gas such as air. The injected fuel stream breaks into drops which begin to vaporize. Numerous models have been developed over the years to predict the behavior of heterogeneous systems (Faeth 1983). Because most of the particles in a typical spray have diameters $> 10\ \mu$m (Kuo 1986), transfer processes between the liquid and gas should be considered. Many models treat the liquid phase in a Lagrangian fashion, while the gas phase is modeled in a Eulerian manner. Correlations are implemented to account for mass, momentum and energy transfer between the phases. While most models employ simple drag laws for the droplets, many models differ in their treatment of the gas phase. Deterministic models neglect the effect of turbulence on drop dispersion, while stochastic simulations account for turbulent intensities and length scales (Kuo 1986).

An approach common to many models of spray processes is the use of a modified particle equation that was originally derived by Bassett and others for Stokes flow. The equation includes a term that accounts for flow unsteadiness, viz. the Bassett term. One of the most complete versions of this equation for low Reynolds number (Re) motion of particles in a nonuniform flow was derived by Maxey & Riley (1983). Corrections for larger Re are usually applied by spray modelers (Faeth 1983), very often with the approach of Odar & Hamilton (1964) who applied a Re and acceleration number correction to the Stokes terms in the equation of particle motion. Although spray modelers adopt this form of the equation, they frequently neglect all effects except drag, following order of magnitude estimates of the relative contributions of the various terms.

In order to examine some of the simplifications commonly made in spray models, the transition region of a jet was modeled deterministically using a vortex dynamics code. A general equation of motion for particles in an unsteady, nonuniform flow was utilized to track the particle's motion. Since the vortex dynamics code was capable of simulating three-dimensional flow fields, the effect of circumferential fluctuations on particle dispersion was examined. Differences in the particle dispersion curve at different pressures and drop diameters were used to determine the importance of the Basset, virtual mass and fluid forces. These forces account for the effect of unsteadiness and nonuniformity of the flow field on a particle's motion. Furthermore, the effect of varporization and the Basset, virtual mass and fluid forces on particle dispersion was investigated under a typical combustor condition of 20 bar and 1500 K.

2. BACKGROUND

Flow field

The predominance of ring-like structures in the transition region of the round jet suggests that this flow can be modeled by periodically releasing rings with small amplitude helical disturbances near the nozzle exit. A numerical simulation of this type of flow can be done in various way but the presence of ring-like structures indicates that vortex dynamics offers the advantage of tracking the relevant parts of the fluid without requiring the discretization of the complete flow field (Chorin 1980; Leonard 1985). The present method is based on the inviscid Navier–Stokes equations written in terms of vorticity ω:

$$\frac{D\omega}{Dt} = (\omega \cdot \nabla)\mathbf{u}, \qquad [1]$$

where

$$\frac{D}{Dt} \equiv \frac{\partial}{\partial t} + (\mathbf{u} \cdot \nabla) \qquad [2]$$

denotes the substantial derivative. The velocity $\mathbf{u}$ follows from the relation

$$\nabla^2 \mathbf{u} = -\nabla \times \omega \qquad [3]$$

and can be given explicitly in the absence of boundaries. If the vorticity is concentrated in thin filaments, then the velocity that is induced by the filaments can be calculated from the Biot–Savart integral obtained by solving [3]. The integral is known to diverge for filaments of zero thickness and the structure of the filaments must be taken into account in order to obtain acceptable values for the induced velocity. Several approximations are available (Chorin 1980; Anderson & Greengard 1984; Leonard 1985) for thin filaments. The present method assumes thin filaments with circular cross sections and employs Rosenhead's method (Leonard 1985; Lundgren & Ashurst 1989), where the integrand is modified to remove the singularity:

$$\mathbf{u}(\mathbf{x}, t) = -\frac{\Gamma}{4\pi} \int_C \frac{[\mathbf{x} - \mathbf{r}(s)] \times \left(\frac{\partial \mathbf{r}}{\partial s}\right)}{(|\mathbf{x} - \mathbf{r}(s)|^2 + \mu^2)^{3/2}} ds. \qquad [4]$$

The circulation of the filament is denoted by Γ and $\mathbf{r}(s)$ is the position of the centerline of the filament with arclength s. The parameter $\mu > 0$ accounts for the structure of the filament in an approximate manner (Leonard 1985). Moore (1972) showed that μ should be proportional to the local core radius σ:

$$\mu = \alpha^{1/2}\sigma \qquad [5]$$

where α is a nondimensional parameter which reflects the vorticity distribution in the core of the filament. For a uniform vorticity distribution, $\alpha \approx 0.22$.

The thin filament approximation that we have used has several limitations. For instance, it predicts excessive growth rates for short-wavelength disturbances and energy is not conserved when core overlap occurs (Ashurst & Meiburg 1988). It simulates the dynamics of inviscid flows and cannot represent the viscous reconnection of filaments which is typical of turbulent flows at high but finite Re. Therefore, the thin filament approximation can be used to represent the vortices that are formed in the initial region of a jet as long as disturbance wavelengths are large and core overlap and viscous reconnection are not significant.

Nonvaporizing particles

The modified BBO equation, due to Basset (1888), Boussinesq (1903) and Oseen (1927), was derived for spheres accelerating at low Re (Stokesian motion). Most gas particle interactions, however, occur at larger Re, where the convective acceleration terms in the Navier–Stokes equation are important. In an effort to incorporate the effect of convective acceleration of the gas surrounding the particle, Odar & Hamilton (1964) modified the Stokes drag, virtual mass and Basset terms. Equation [6] illustrates the modifications made by Odar & Hamilton (1964). The

derivatives d/dt_p and D/Dt_G appearing [6] were taken following the particle and the gas, respectively:

$$\frac{d\mathbf{u}_p}{dt} = \frac{3C_D}{4d}\frac{\rho_G}{\rho_p}|\mathbf{u}_G - \mathbf{u}_p|(\mathbf{u}_G - \mathbf{u}_p) + \frac{1}{2}\frac{\rho_G}{\rho_p}C_I\frac{d}{dt_p}(\mathbf{u}_G - \mathbf{u}_p) + \frac{\rho_G}{\rho_p}\frac{D\mathbf{u}_G}{Dt_G}$$
$$+\frac{9}{d}\frac{\rho_G}{\rho_G}\left(\frac{\nu}{\pi}\right)^{1/2}C_B\int_{t_0}^{t}\frac{\dfrac{d(\mathbf{u}_G - \mathbf{u}_p)}{dt_p}}{(t-\tau)^{1/2}}dt + \left(\frac{\rho_G}{\rho_p} - 1\right)\mathbf{g}, \quad [6]$$

where C_D, C_I and C_B are the drag, virtual mass and Basset coefficients, respectively. Subscripts p and G refer to the particle and gas phase respectively. The densities of the particle and the gas are represented by ρ_p and ρ_G. Generally, C_I and C_B are functions of the particle Reynolds number, Re, and the acceleration number, An, defined below (Faeth 1983):

$$\mathrm{Re} = \frac{|\mathbf{u}_G - \mathbf{u}_p|d}{\nu} \quad [7]$$

and

$$\mathrm{An} = \frac{\left|\dfrac{d(\mathbf{u}_G - \mathbf{u}_p)}{dt_p}\right|}{|\mathbf{u}_G - \mathbf{u}_p|^2}d. \quad [8]$$

The kinematic viscosity of the gas is ν and the particle diameter is d. Odar & Hamilton (1964) found that the functions C_I and C_B were functions of An only for the conditions of their experiments, i.e. $\mathrm{Re} < 62$ and for a simple harmonic motion. Correlations for C_D (Putnam 1961), C_I and C_B (Odar & Hamilton 1964) are given below:

$$C_D = \frac{24}{\mathrm{Re}}\left(1 + \frac{\mathrm{Re}^{2/3}}{6}\right) \qquad \mathrm{Re} < 1000, \quad [9]$$

$$C_I = 2.1 - \frac{0.132\,\mathrm{An}^2}{(1 + 0.12\,\mathrm{An}^2)} \qquad \mathrm{Re} < 62 \quad [10]$$

and

$$C_B = 0.48 + \frac{0.52\,\mathrm{An}^3}{(1 + \mathrm{An})^3} \qquad \mathrm{Re} < 62. \quad [11]$$

Using [6]–[11], the non-Stokesian motion of a rigid, spherical particle in a unsteady, nonuniform flow can be tracked deterministically. Athough simplified forms of this equation widely applied to spray calculations some potential uncertainties should be indicated.

Some theoretical objections to the BBO equation can be raised. For example, on the basis of an asymptotic analysis of the unsteady Navier–Stokes equation, Ockendon (1968) pointed out that unless the time scale of the unsteadiness was sufficiently large, then an expansion in terms of Re was invalid. For a 50 μm dia drop in air, the time scale of the unsteadiness would need to be of the order of $10^{1/2}$ μs or less in order for this situation to pertain. For the time scales that we might encounter in the jet flow, the usual unsteady Stokes solution will be valid at small Re.

However, at higher Re the situation is uncertain. The Re values in the present simulations span a large range and fluctuate with time. The smallest Re are encountered with the 25 μm droplets. Their Re values do not rise above about 5. For all other cases, except 150 μm droplets at 20 bar, Re values vary between 0–30. The largest Re values occur with the 150 μm drops at 20 bar. Near the nozzle these drops exhibit Re values of around 50–80 and further downstream the Re values vary between 100–200.

Although the modified BBO equation with the coefficient of Odar & Hamilton (1964) is widely used in spray models, its validity, in particular the unsteady terms, is not generally accepted. Clift *et al.* (1978) state that there is no *a priori* justification for the use of an equation of the form of [6]. However, they cite data from experiments on droplets falling from rest in a quiescent fluid which indicate that a reasonably good agreement with [6] can be achieved. Odar (1966) arrived at a similar conclusion. On the other hand, Karanfilian & Kotas (1978) found that the modified unsteady

Stokes equation did not correlate their experimental data very well. Their experiments examined the forces on a sphere in an oscillating flow at moderately high Re. It seems that the nature of the flow plays some role in determining the validity of [6]. The simulations that are presented here combine aspects of both flow situations. The particles are released with a velocity that matches that of the flow field. Further downstream, the turbulence may tend to approximate a simple harmonic motion. Therefore, some uncertainty surrounds the precision of the various terms in the modified BBO equation as a result of Re values that are significantly >1. Nevertheless, given the wide use of this equation in spray models, it is worth examining the importance of each term under realistic turbulent conditions.

Vaporizing particles

Most heterogeneous spray applications occur at elevated temperatures, where the effect of vaporization on drag must be considered. Yuen & Chen (1976) found that vaporization affects drag in two ways. First, the temperature and concentration gradients between the drop surface and the ambient gas cause substantial reductions in the absolute viscosity of the gas, which decreases friction drag. Second, vaporization affects the boundary layer surrounding the drop. This effect, called "blowing", reduces friction drag and increases form drag. In order to account for both variable properties and blowing, Renksizbulut & Yuen (1983) proposed the following correlation for the drag coefficient:

$$C_{Dv} = \frac{24}{Re_m}(1 + 0.2\,Re_m^{0.63})(1 + B_f)^{-0.2} \qquad 10 < Re < 300, \qquad [12]$$

where Re_m and B_f are the mean Reynolds number and the mass transfer number at the film condition, respectively. The mean mass transfer number is

$$B_f = \frac{C_{pf}(T_\infty - T_s)}{L_s}, \qquad [13]$$

where L_s is the latent heat of vaporization of the drop at surface temperature T_s and C_{pf} is the specific heat of the vapor and air mixture at the film condition. The mean kinematic viscosity, v, is equal to μ_f/ρ_∞, where ρ_∞ is the density of the gas at temperature T_∞ at infinity, and μ_f is the absolute viscosity of the vapor and gas mixture at the film condition.

The droplet diameter, d, is a function of time and is calculated using

$$\frac{d(d)}{dt} = \frac{\dfrac{2\,dm}{dt}}{\pi\rho_p d^2}, \qquad [14]$$

where m is the instantaneous particle mass. Balancing the heat transfer by convection to the drop surface with the heat required to vaporize the drop, the rate of change of particle mass with time is given by

$$\frac{dm}{dt} = \pi d\,Nu_f k_f \frac{(T_s - T_\infty)}{L_s}, \qquad [15]$$

where Nu_f and k_f are the Nusselt number and thermal conductivity at the film condition, respectively. Equation [15] was obtained by assuming that the temperature in the drop was T_s and invariant in both space and time. Finally, Renksizbulut & Yuen (1983) developed a correlation for Nu_f:

$$Nu_f = (2 + 0.57\,Re_m^{0.5}\,Pr_f^{0.33})(1 + B_f)^{-0.7} \qquad 10 < Re_m < 2000, \qquad [16]$$

where Pr_f is the Prandtl number evaluated at the film condition. Using [6] and [12]–[16], the non-Stokesian motion of a vaporizing drop in a unsteady, nonuniform flow can be tracked.

3. METHODS

Normalized variables

In order to generalize the flow computation, all length scales, velocities and times were nondimensionalized by the jet radius, R, the jet exit velocity, U_e, and R/U_e, respectively. Thus, the

circulation, Γ, in [4] was nondimensionalized by U_e and R. In all sections where the flow field is discussed, the flow field parameters will be in nondimensional form unless otherwise specified. Variables for the particle computations were left in a dimensional form to reduce the complexity of the discussion.

Flow field

The transition region of a 0.0254 m dia air jet with an Re_D of approx. 30,000, as in Crow & Champagne (1971), was modeled both axisymmetrically (no azimuthal disturbances) and three-dimensionally. To reproduce the large-scale behavior of the transition region, a model was utilized which consisted of upstream, transition and downstream regions. The upstream region simulated the effect of the flow field in the nozzle on the transition region's vortices; it extended from a nondimensional axial distance of 2 inside the nozzle to the nozzle tip. The downstream region contained large axisymmetric vortices which were formed by combining the distorted groups of vortices at the end of the transition region. These large vortices had approximately the same effect on the transitional vortices as the original group, but required less computational effort. The computational time in the axisymmetric simulation was at least an order of magnitude less, so combination was unnecessary.

Nonvaporizing particles

Equations [7]–[11] and [17] were used to solve for the trajectory of a nonvaporizing, rigid sphere

$$\frac{d\mathbf{x}_p}{dt} = \mathbf{u}_p, \qquad [17]$$

in which $\mathbf{x}_p$ is the particle position.

The gas velocity was calculated by summing [4] over all filaments in the upstream transition and downstream regions. The derivatives appearing in [6] were estimated using first-order differences for both temporal and spatial derivatives. A spatial increment of $10^{-4}R$ (R is the jet radius) was chosen because it provided satisfactory convergence of the spatial derivatives, while the temporal increment was based on the flow time step. The air density was evaluated using the ideal gas equation of state and the particle density was assumed to be constant. The kinematic viscosity in [6] and [7] was computed using the air density and a temperature-dependent correlation for the absolute viscosity of air. The gravitational constant was 9.81 m s^{-1} and acted along the jet axis. The jet flowed downwards.

Equations [6] and [17] were solved for $\mathbf{x}_p$ using an SPC (simple predictor–corrector) method in the three-dimensional jet simulation and an APC (Adams predictor–corrector) method in the axisymmetric jet simulation. The same flow time step was used in both methods and an SPC was used to start the APC. Since both the SPC and APC methods had implicit correctors, the determination of the particle acceleration, $d\mathbf{u}_p/dt$, at the next time $t + \delta t$ was necessary. However, this was not straightforward since the fourth term on the right-hand side of [6] was singular at $\tau = t$. Furthermore, this term contains $d\mathbf{u}_p/dt$ under the integral sign, making [6] implicit in $\mathbf{u}_p$. The particle's acceleration was taken as a linear function whose slope was computed from its acceleration at τ and $\tau - \delta t$. Corrections were repeated until the difference between the corrected acceleration and the previous acceleration was within 0.1%.

The effect of circumferential fluctuations on particle dispersion was examined using rigid, 50 μm particles in a 1 bar, 300 K, air jet. The jet was modeled three-dimensionally, and its density, absolute viscosity, exit velocity and diameter were 1.18 kg m^{-3}, 1.85×10^{-5} kg m^{-1} s^{-1}, 16.6 m s^{-1} and 0.0254 m, respectively. The particles each had a density of 700 kg m^{-3} (octane's density at 300 K) and were released at axial and radial coordinates of $1.0R$ and $0.7R$, respectively. At this point the turbulence intensity was low, ensuring approximately the same initial Re for all particles. To impose as little slip as possible, the particles were released at the jet exit velocity. One particle was released into the flow field at a period of roughly 0.04 from a time of 25, until 213 particles were released. Only the drag and buoyancy forces were included in the force balance for the three-dimensional case in order to reduce the computational effort. Finally, the importance of circumferential fluctuations on particle dispersion was qualitatively examined by visually comparing circumferential dispersions to radial dispersions at the end of the transition region.

The effects of the virtual mass, Basset, fluid and buoyancy forces on particle dispersions were examined with the axisymmetric calculation using the particle density, initial particle position and air absolute viscosity discussed in the previous paragraph. Six cases were run using different diameters and gas pressures. Elevated pressures introduce some additional complexities in that a number of variables change values, e.g. density and kinematic viscosity. Therefore, we have chosen to maintain a constant jet momentum and diameter of 323 N m^{-2} 0.0254 m, respectively. Thus, as the pressure increased, the jet exit velocity decreased and Re_D increased. However, the structure of the transition region, as given by its instability wavelength and boundary layer thickness, was held constant even though its length normally decreases with increasing Re_D (Yule 1978). The transition region's structure was not changed in order to reduce the number of variables in the problem and the computational complexity.

Three of the cases were run at 1 bar, $\nu = 1.5716 \times 10^{-5}$ m^2 s^{-1} and $U_e = 16.56$ m s^{-1}, with particle diameters of 25, 75 and 150 μm. Additionally, three cases were run at 20 bar, $\nu = 7.8578 \times 10^{-7}$ m^2 s^{-1} and $U_e = 3.70$ m s^{-1} with the same particle diameters as used in the 1 bar cases. In each case, two particles were released at alternate time steps. The first particle's force balance had only drag and buoyancy forces (termed the type I method), while the second particle's force balance included drag, buoyancy, virtual mass, Basset and fluid forces (termed the general method). The particles were released into the flow starting from a time of 30 because the flow in the jet's transition region was sufficiently steady after this time. Finally, each particle was allowed to interact with the flow for a period of 20, giving the particles enough time to pass through the transition region. The effects of the virtual mass, Basset and fluid forces were found by comparing dispersion curves for the type I and general methods. Furthermore, the importance of these forces and the buoyancy force relative to the drag force was examined by comparing the ratio of the average Basset, virtual mass, fluid and buoyancy forces to the average drag force for the first particle released in each of the six cases.

Vaporizing particles

The same set of equations were solved for vaporizing droplets with the addition of the mass transfer calculations. The evaluation of fluid properties, however, was more difficult in the vaporizing case due to the concentration and temperature gradients in the boundary layer. Gas properties were found in White (1984) and Beaton & Hewitt (1989) for octane at 1500 K and 20 bar. The thermal conductivity and absolute viscosity of the air–octane mixtures at film conditions were derived using mixing relationships that may be found in Kanury (1975). Gas densities were evaluated using the Hankin–Brobst–Thomson technique (Reid *et al.* 1987).

To examine the effect of vaporization on particle dispersion and on the virtual mass, Basset, fluid, drag and buoyancy forces, vaporizing octane particles were released into a 1500 K, axisymmetric air jet whose efflux of momentum was 323 N m^{-2}. A typical combustor pressure of 20 bar was used. The particle release rate, initial location, time of flight and data analysis were the same as used for the nonvaporizing particles. The particles initial velocity was also equal to the jet exit velocity. The particle diameter was initially 150 μm and it was removed from the flow field when its diameter was < 10 μm.

Statistics

In the three-dimensional simulation, both the flow field and particle computations were performed simultaneously. The flow field and particle computations were not performed separately because the storage requirements for the three-dimensional flow field were greater than the available resources. In the three-dimensional jet simulation, root-mean-square (RMS) velocity, Reynolds stress and mean velocity profiles at axial locations of $1.0D$, $2.0D$ and $3.0D$ were determined to evaluate the jet model. The trapezoidal rule was used for averaging, and the jet exit velocity was used as a normalizing factor for all statistical values. The axial, radial and circumferential velocities were sampled every time step and a nondimensional time of 25–40 giving 565 samples.

In order to compute the radial dispersion of a group of N particles at a time of flight, t_f (s), we used

$$D_R(t_f) = \frac{\sum_{j=1}^{N} [r_j(t_f) - r_j(0)]^2}{N}, \qquad [18]$$

where D_R is the radial dispersion in mm^2, r_j is the radial location of the jth particle in mm at t_f and $r_j(0)$ is the initial radial location of the jth particle; 250 particles were used at each time of flight. It should be recalled that the vortex dynamics calculation is not a stochastic simulation and, therefore, the term "statistics" is applied in the sense that an adequate number of particle must be used to define the behavior within one or two of the large vortices. Many more particles will only provide redundant information. In fact, some calculations were performed with twice the number of particles and the dispersion was found to change by $< 1\%$. For example, the dispersion of 250 particles (50 μm dia and 1 bar pressure) at long times of flight ($x/D \approx 10$) was 207 mm^2; the dispersion of 500 droplets under identical conditions was 210 mm^2.

To determine the ratio of the average virtual mass, fluid, Basset and buoyancy forces to the average drag force, dot products of $d\mathbf{u}_p/dt$ with each of the terms on the right-hand side of [6] were taken. This gave the instantaneous value of each term in the direction of $d\mathbf{u}_p/dt$. The magnitude of each term was averaged using the trapezoidal rule until the particle had passed a particular axial location which was chosen to ensure that all particles followed approximately the same path. The averaged Basset, virtual mass, fluid and buoyancy terms were then divided by the averaged drag term to give a force ratio. This force ratio could be used to determine the importance of the Basset, virtual mass, fluid and buoyancy forces in comparison to the drag force.

4. RESULTS AND DISCUSSION

Flow field

Figures 1(a–f) illustrate the temporal and spatial development of the vortices in the three-dimensional simulation of the transition region. The thickness of the vortices is not shown in the pictures. These pictures show how the vortices coalesce and the helical disturbances grow and entangle as time progresses. Three coalescing regions are present from $0.5D$ to $3.5D$, which agrees with the observations made by Yule (1978). The first combination occurs at approx. $1D$, as shown by the 2 rings at $1.0D$ in figure 1(a). This group then combines with either 1, 2 or 3 rings to form a group of 3–5 rings, as illustrated by the groups centered at $1.75D$ and $1.5D$ in figures 1(a) and (c), respectively. The final combination involves groups of 3–5 vortices and occurs between $2D$ and $3.5D$. This coalescence is illustrated in figure 1(c), where the groups at $1.75D$ and $2.5D$ in figure 1(a) come together at $3.0D$. The large group located at $3.5D$ in figure 1(e) is the result of the this last combination and corresponds to the puffs of smoke which were observed in Crow & Champagne's (1971) jet.

Test of the particle method

To test the method for solving [6] and [17] numerically, a theoretical solution of [6] for a uniform flow undergoing oscillatory motion with a frequency ω was utilized (Hjelmfelt & Mockros 1966). This solution of [6] was based on a Stokesian interaction between the particle and the gas ($C_D = 24/\mathrm{Re}$, $C_B = 1$, and $C_I = 1$), where buoyancy was neglected. Hjelmfelt & Mockros (1966) discussed three types of approximations: approximation I neglected the Basset term; approximation II neglected both the Basset and virtual mass terms; and approximation III only included Stokes drag. In their analysis they made comparisons of the effect of the various approximations on the phase lag and amplitude response between the particle and gas velocities. Figure 2 illustrates a comparison of the present numerical scheme and theoretical solutions of [6] for $\rho_p/\rho_G = 20.0$. The abscissa of figure 2 is the Stokes number, $N_S = (\nu\omega^{-1}d^{-2})^{1/2}$. This graph illustrates the excellent comparison between the numerical and theoretical solutions for all cases, including the general case where all terms are included. Figure 2 also illustrates that approximation I (neglecting the Basset term) produces deviations from the general case for most Stokes numbers.

Although this test does not evaluate the spatial derivatives, the buoyancy term, C_I, C_B and C_D, it does test many of the methods used to solve [6] and [17], including those used to solve the Basset term. Computing the implicit and singular Basset term was considered the major difficulty in the solution of [6].

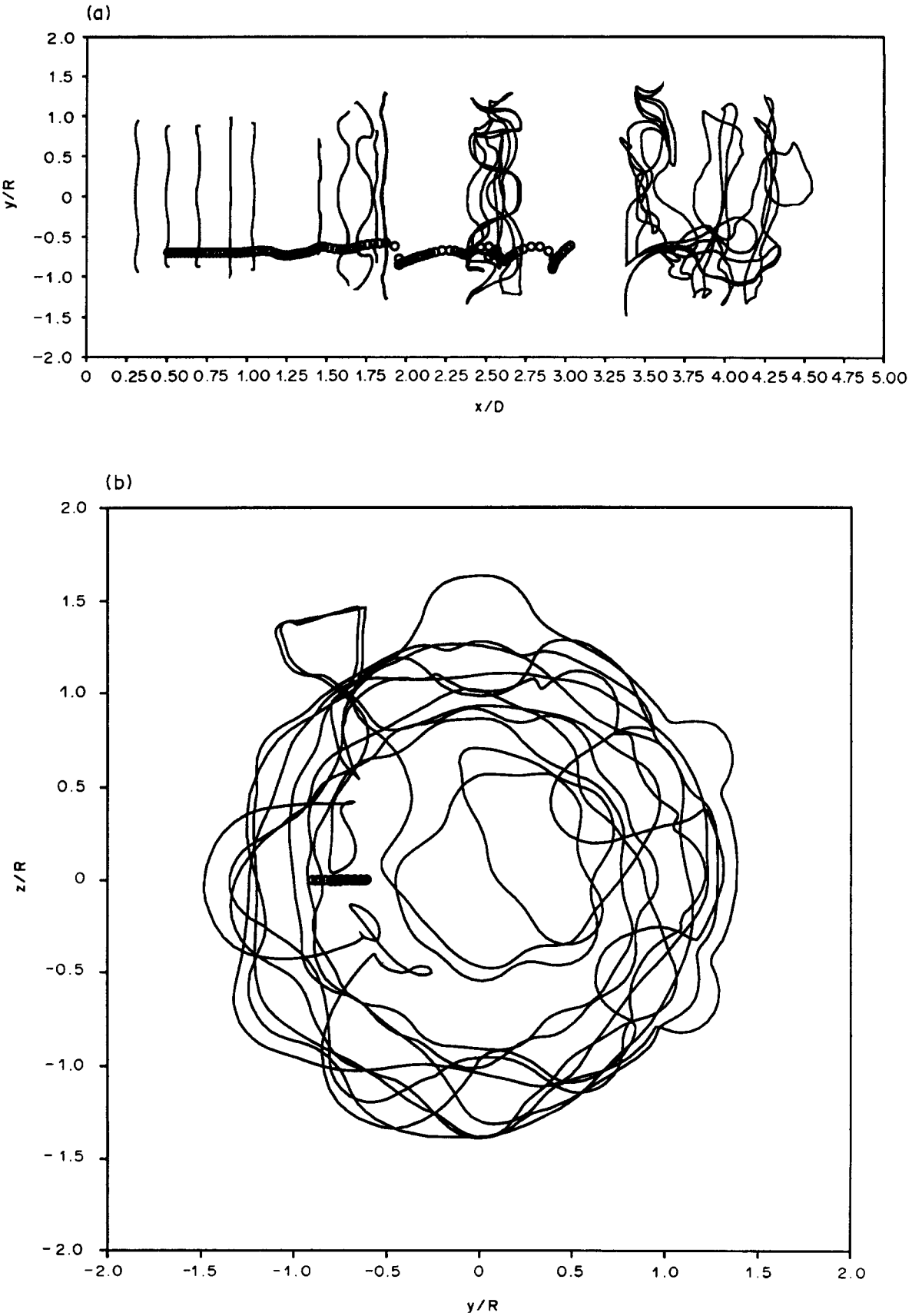

Figure 1—*legend on p. 568.*

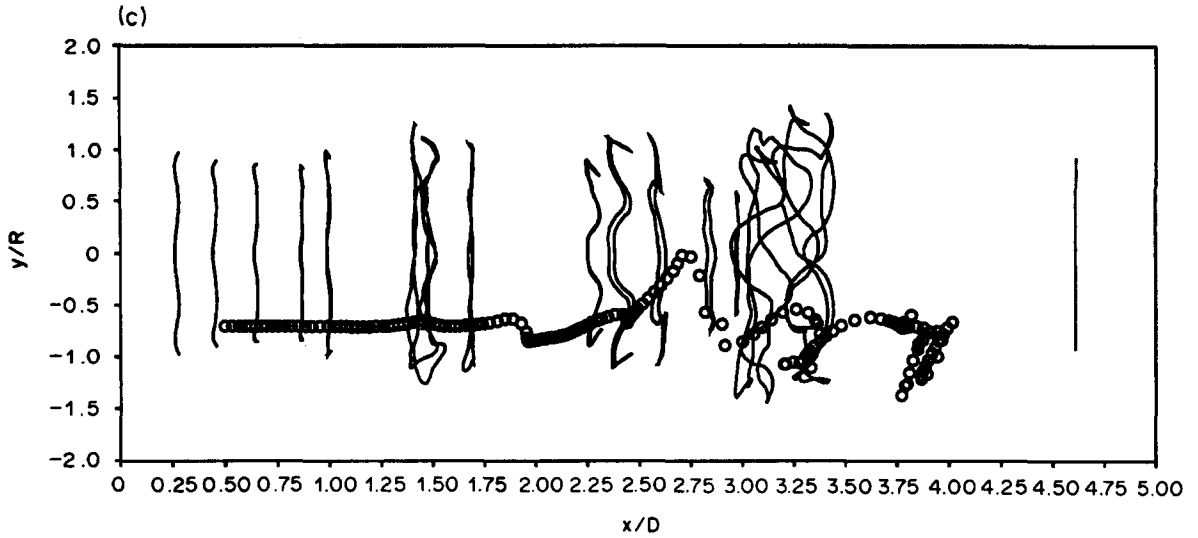

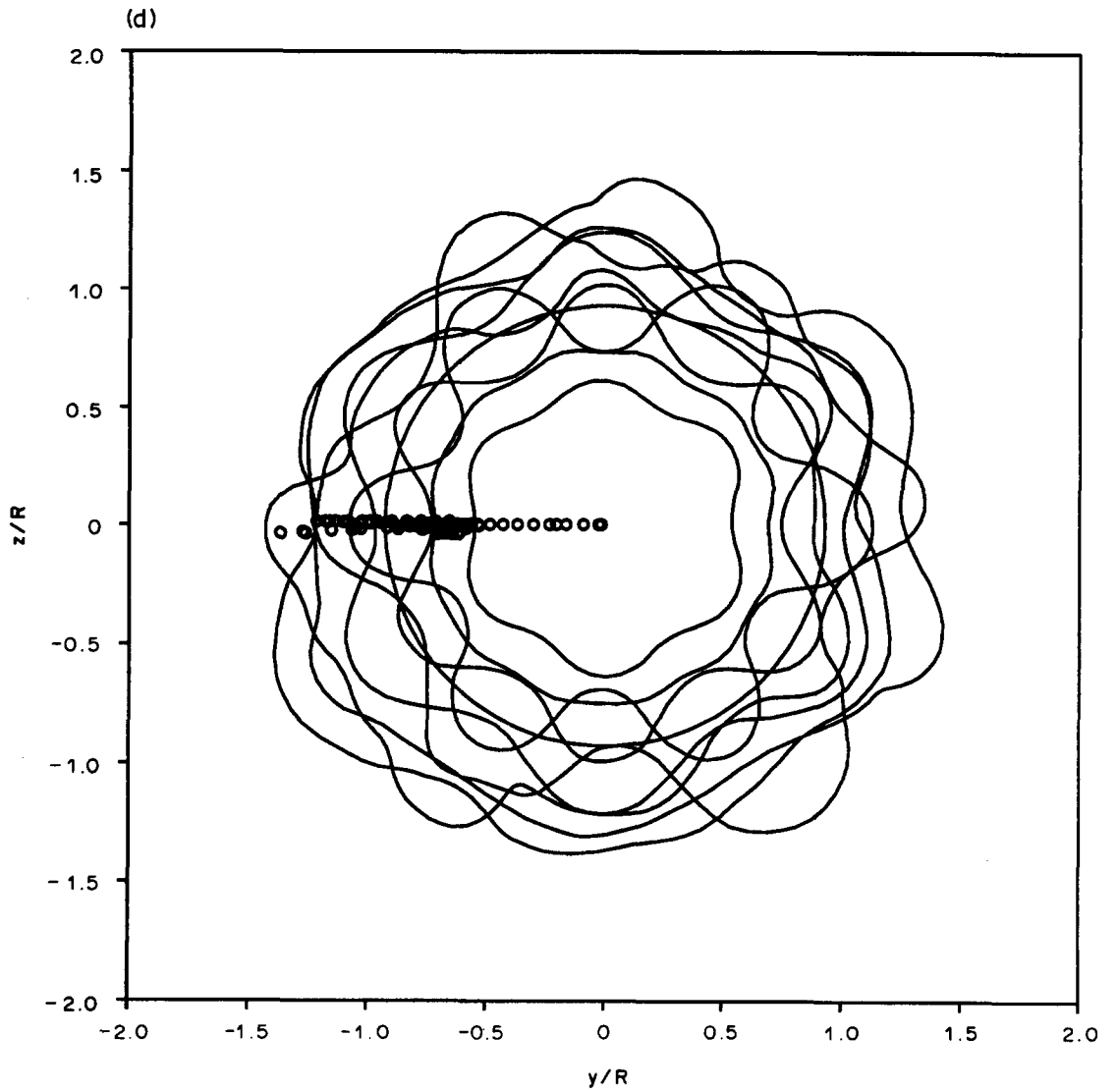

Figure 1—*legend overleaf.*

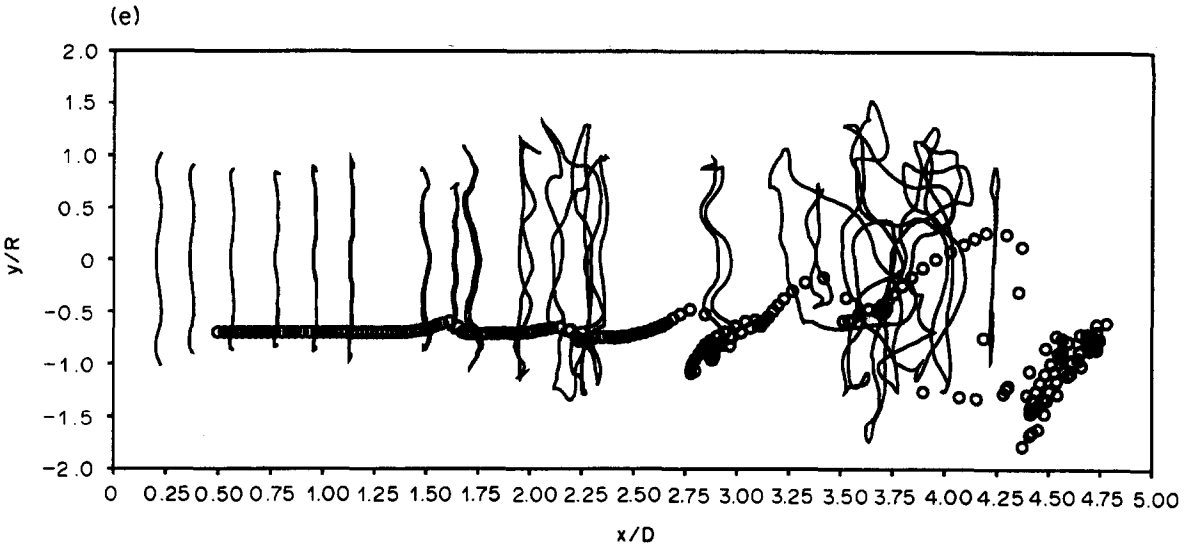

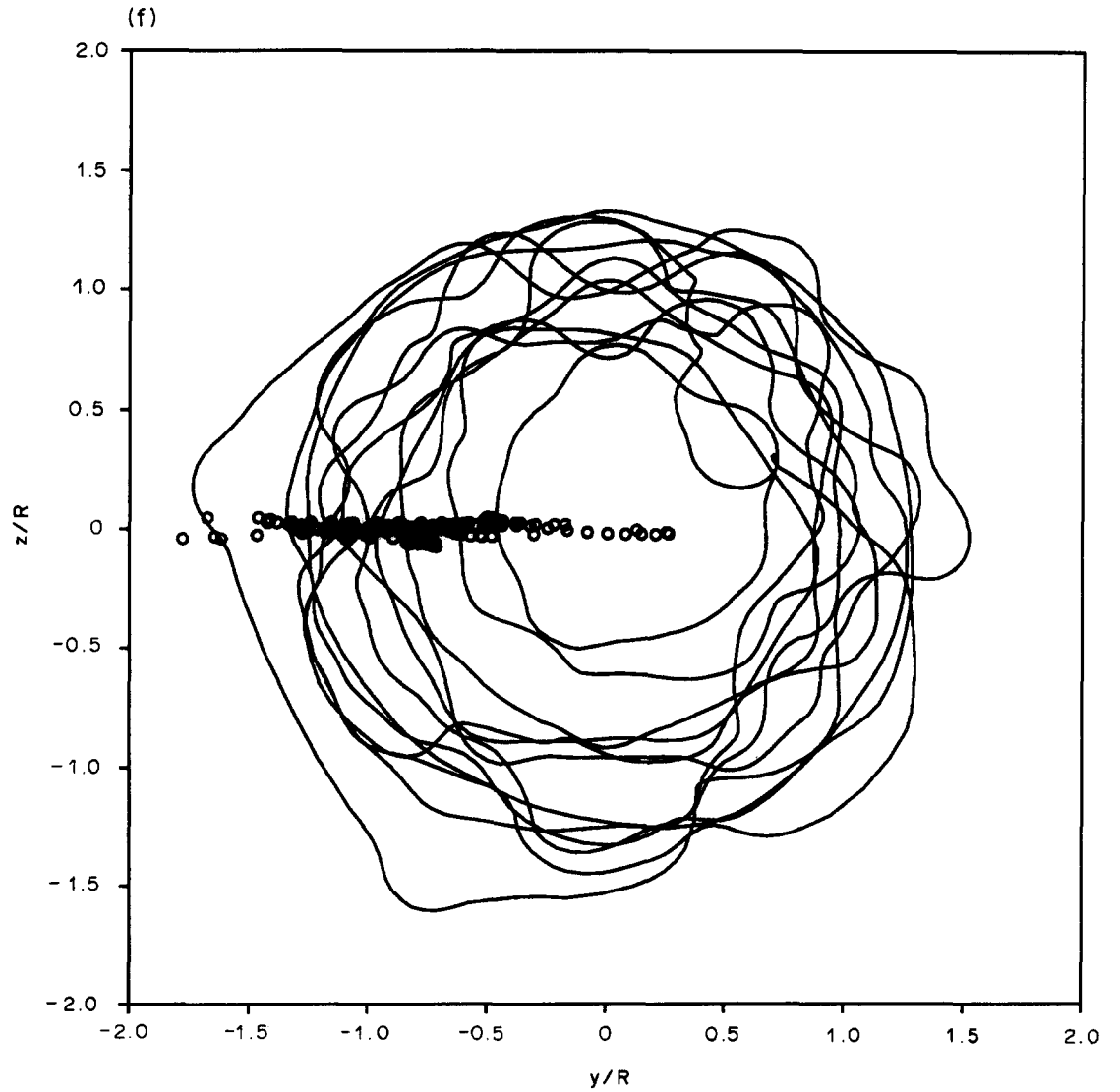

Figure 1(a–f). Circumferential and radial dispersion of rigid, 700 kg m^{-3}, 50 μm particles at 1 bar in 300 K air at nondimensional times: (a, b) 30.75; (c, d) 33.77; (e, f) 36.72. Particles are shown as circles, vortices as lines.

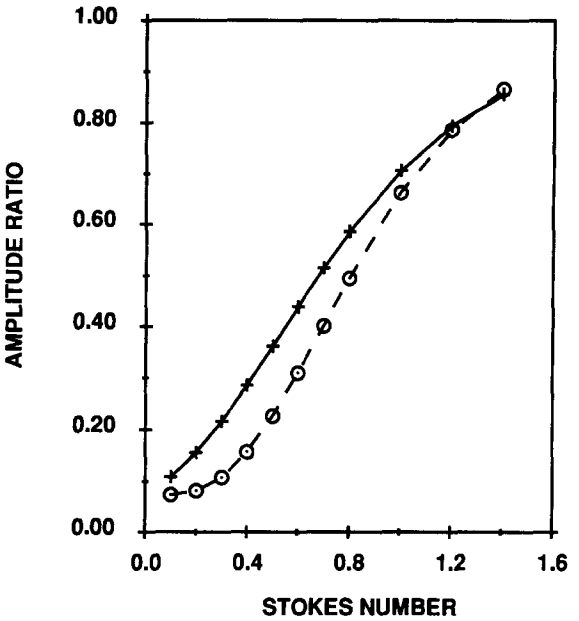

Figure 2. Comparison of the numerical and theoretical solutions of the droplet equation of motion for the velocity amplitude ratio of a discrete particle in a uniform, oscillatory flow. Density ratio of 20. +, Numerical solution of the general equation; ——, theoretical solution of the general equation; O, numerical solution with the type I approximation; – – –, theoretical solution with the type I approximation.

Circumferential dispersion

Figures 1(a–f) illustrate both radial and circumferential particle dispersion in the three-dimensional simulation of the transition region. In the figures, x, y and z are the axial, radial and circumferential coordinates, respectively. Figures 1(a, c, e) are side views of the vortices and particles at several different times. Figures 1(b, d, f) are frontal views of the same vortices and particles in the axial range from $2.0D$ to $5.0D$ at the same time. Figures 1(c, e) indicate that the final coalescence and the large group of rings that results are primarily responsible for the radial dispersion of particles. As the group of 5 rings at $1.75D$ in figure 1(a) passes through the rings at $2.5D$, it accelerates both axially and radially. A few of the particles are pulled along, as seen in figure 1(c) at $2.5D$. Most are left behind, however, due to their inertial resistance to fluid accelerations, as indicated by the group of particles at $3.0D$ in figure 1(e). Because the fluid velocity in the region between the large groups of vortices is small, the group of particles at $3.0D$ in figure 1(e) will decelerate. This group will then be dispersed radially away from the jet by the group of vortices at $2.0D$ in the same figure, like the group of particles at $4.5D$. From this observation a two-step process for particle dispersion in the transition region may be postulated. In the first step, particles are stranded by the final coalescence in the regions of low velocity behind and in front of the coalescing rings. These stranded groups of particles are then dispersed radially away from the jet by the next passing group of vortices.

Figures 1(b, d, f) indicate that the circumferential dispersion of particles is insignificant down to at least $5.0D$. The result is not surprising since both the mean and RMS circumferential velocities are small, indicating that the instantaneous circumferential velocities are small. The simulations produced circumferential turbulence intensities (relative to the jet exit velocity) of around 5% at $20D$. The radial intensities were considerably higher, in accord with the results of Yule (1978) who found that the two components did not approach each other to within 15% until about $4.0D$ downstream. Furthermore, the time scale of the circumferential fluctuations is small, giving the particles little time to develop appreciable circumferential velocity.

Basset, virtual mass, fluid and buoyancy forces

Figures 3(a) and (b) illustrate the effect of drop diameter and the type I approximation on radial dispersion at 1 and 20 bar, respectively. These figures show that dispersion levels off as the time

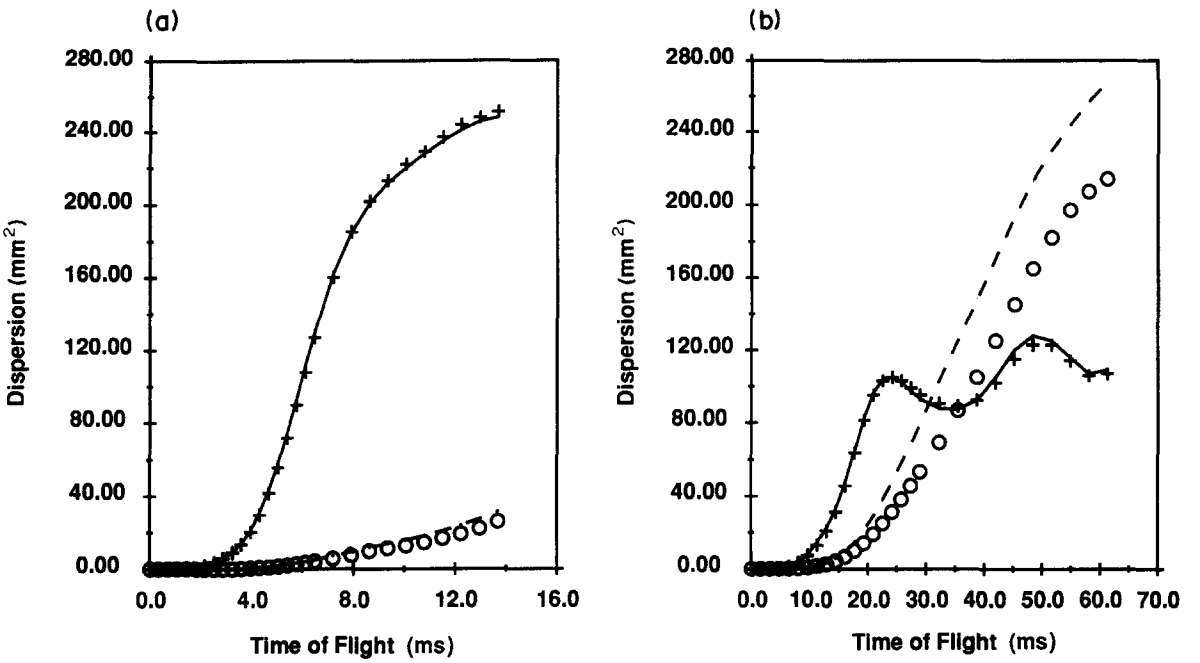

Figure 3. Effect of particle diameter, pressure and the type I approximation on radial dispersion of rigid, 700 kg m^{-3} particles in 300 K air at pressures of: (a) 1 bar, (b) 20 bar. —, $D_p = 25\ \mu m$, general equation; +, $D_p = 25\ \mu m$, type I approximation; – – –, $D_p = 150\ \mu m$, general equation; ○, $D_p = 150\ \mu m$, type I approximation.

of flight becomes large for the 25 μm dia particles at 1 bar and all particle types at 20 bar. Dispersion levels off for these particles because they are briefly captured by the large groups of vortices at the end of the transition region and are dispersed or flung to regions beyond the mixing layer where the jet momentum is small (Chung & Troutt 1988). This process is identical to the two-step procedure discussed under *Circumferential dispersion* above, where particles are stranded in the low-velocity regions in front of and behind the last coalescence and then pushed away from the jet by the next passing groups of vortices. Figures 4(a–c) illustrate the 25, 75 and 150 μm particle locations at the last time of flight at 1 bar for the general case, while figures 5(a–c) show the last time of flight at 20 bar.

Chung & Troutt (1988) found that particles which were dispersed beyond the mixing layer in the region of the last coalescence had γ-values of order 1, where γ is the ratio of the particle aerodynamic response time, $\tau_p = \rho_p d^2/18\ \mu$, to the flow characteristic time scale, $\tau_G = D/U_e$. Chung & Troutt's (1988) observation was verified at 1 bar for the cases studied here. At 20 bar, however, the 150 μm dia particles whose value of γ was not of order 1 ($\gamma = 6.86$ for the 150 μm dia particles at 20 bar) were also flung from the jet by the last coalescence, as illustrated in figure 5(c). This was a result of the fact that these particles had average Re values which were well beyond Stokes range due to the flow's kinematic viscosity. Since τ_p was derived assuming Stokes flow, it is reasonable to expect that γ is an invalid indicator of particle dispersion behavior at high pressures, especially for the large particles.

The quasi-linear dispersion curves for the 75 and 150 μm dia particles in figure 3(a) indicate that these particles are not dispersed beyond the mixing layer. This is further illustrated in figures 4(b) and (c), which show that the 75 and 150 μm particles travel downstream in large groups and are not thrown from the jet in the region of the last coalescence. According to Chung & Troutt (1988), $\gamma = 7.7$ and 30.8 for the 75 and 150 μm particles at 1 bar. Therefore, they have little time to react to the large structures at the end of the transition region.

Figure 5(c) illustrates that roughly three-quarters of the 150 μm dia particles at 20 bar are dispersed beyond the mixing layer, while one-quarter remain in the jet. Furthermore, comparing figures 4(b) and 5(c) for the 75 μm particles at 1 bar and the 150 μm particles at 20 bar, it is seen that the dispersion behavior is clearly different, even though these particles have similar γs. Once

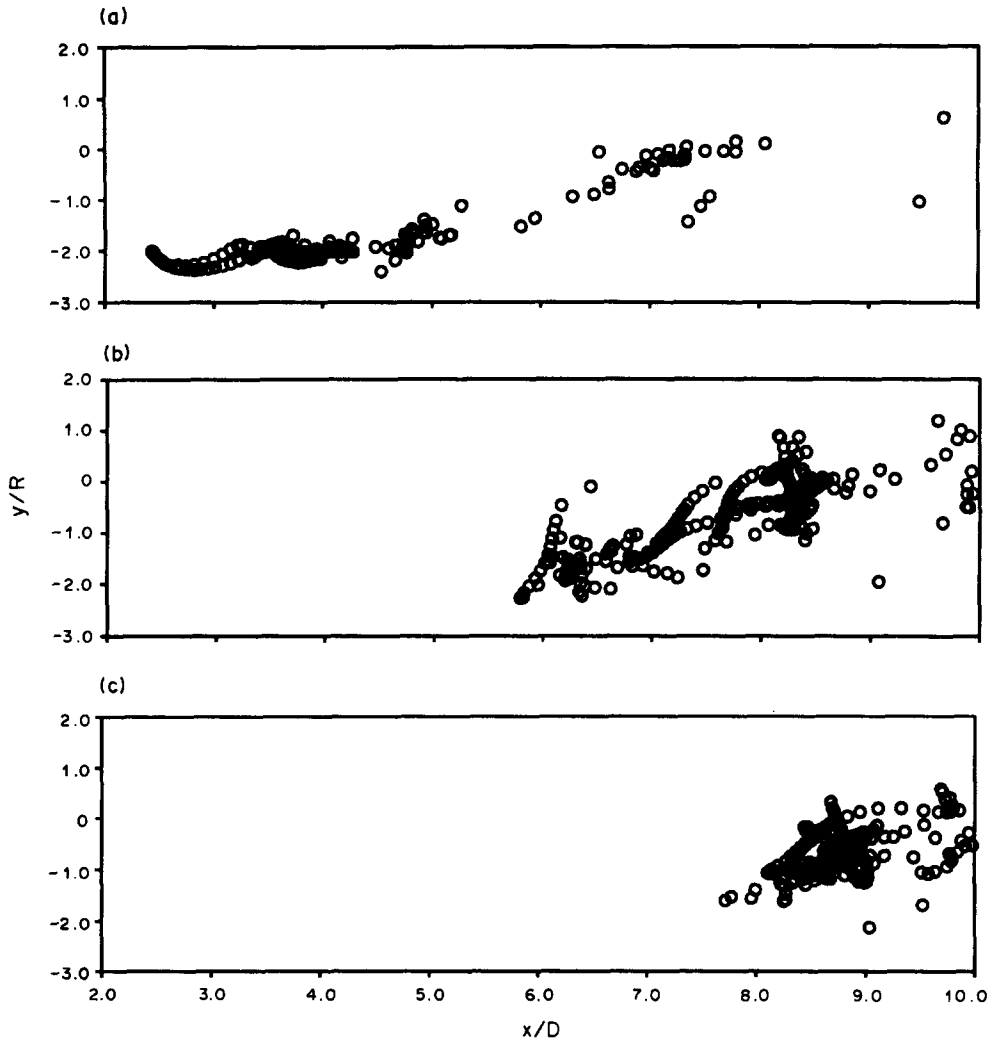

Figure 4. Particle locations at the last time of flight shown in figure 3(a) for the general equation for particle diameters of: (a) 25 μm; (b) 75 μm; (c) 150 μm.

again this illustrates that the use of γ as an indicator of whether the particles will be dispersed beyond the mixing layer or remain in the jet is only valid at low pressures or when the particle Re is small.

Comparing the type I approximation to the general case in figures 3(a, b) for each particle size, it can be seen that the inclusion of the Basset, virtual mass and fluid forces has little effect on the shapes of the dispersion curves. The type I approximation, however, underpredicts dispersion slightly at all flight times for the 75 and 150 μm particles at 1 bar, as illustrated in figure 3(a). For the 150 μm dia particles at 20 bar, dispersion is underpredicted by the type I approximation at all times of flight investigated. Figures 6(a, b) illustrate the relative difference between dispersion predicted by the type I approximation and that given by the general case for each particle size. These figures show that neglecting the Basset, virtual mass and fluid forces can cause significant errors in dispersion at both low and high pressures, especially for large particles.

The largest relative differences between the type I approximation and the general case occur when the time of flight ranges from 0.0 to 0.002 s at 1 bar and from 0.0 to 0.01 s at 20 bar, as shown in figures 6(a) and (b), respectively. In these ranges, the particles are within 2.0D of the nozzle where the drag force is low (and the Re values are low) and the frequency of relative motion between the particle and the gas, f_r, is high. When f_r is high, the Basset, virtual mass and fluid forces can be large (Hjelmfelt & Mockros 1966; Lazaro & Lasheras 1989). The combination of large Basset,

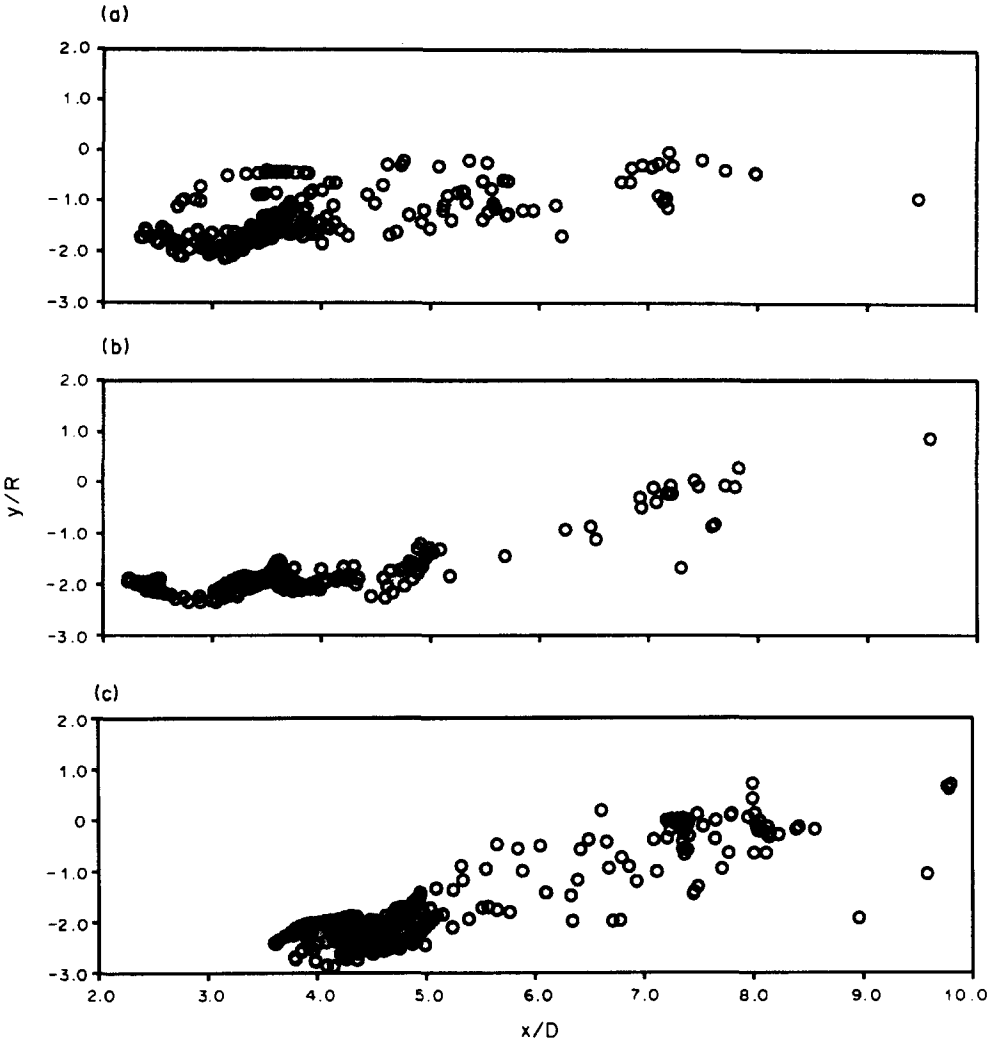

Figure 5. Particle locations at the last time of flight shown in figure 3(b) for the general equation for particle diameters of: (a) 25 μm; (b) 75 μm; (c) 150 μm.

virtual mass and fluid forces and small drag force explains why the relative difference between the type I and the general case is large in the near-nozzle region. Comparing figures 3(a) and 6(a), and figures 3(b) and 6(b), it can be seen that even though the error incurred using the type I approximation is high at small flight times or in the near-nozzle region, dispersion is also low. This indicates that neglecting the Basset, virtual mass and fluid forces will cause, in fact, little error in the actual value of dispersion in the near-nozzle region.

The results that were presented in the previous paragraphs indicate that the inclusion of the Basset, virtual mass and fluid forces in a particle's force balance is most important for large particles at both 1 and 20 bar. This result is not surprising in view of the relative orders of magnitude of the various terms. However, the potential error has been quantified for the first time with this simulation and shown to be around 40% in terms of the dispersion. An analysis of the average magnitude of the various additional forces compared to the drag force showed that the Basset force was the dominant term at 1 atm but at 20 atm the fluid, buoyancy and virtual mass forces were of comparable importance to the Basset force, especially for the larger particles.

Vaporizing particles

Figure 7 shows the effect of the type I approximation on radial dispersion for vaporizing, 150 μm, octane particles in 1500 K air at 20 bar. Particles disperse parabolically up to a flight time of 6.5 ms. After this time the dispersion curve becomes nonparabolic because the particles are undergoing

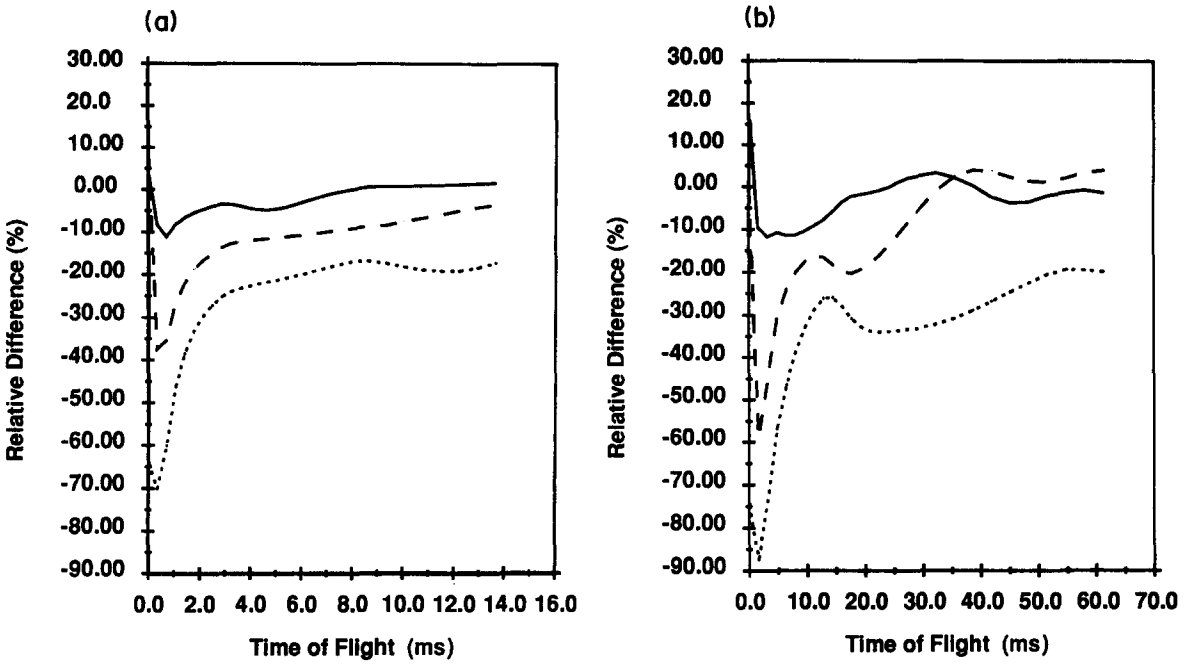

Figure 6. Relative differences between type I and general dispersion calculations for pressures of: (a) 1 bar; (b) 20 bar. ——, $D_p = 25\,\mu$m; – – –, $D_p = 175\,\mu$m; ·····, $D_p = 150\,\mu$m.

complete vaporization (complete vaporization was determined to occur when the particle diameter was $< 10\,\mu$m), as illustrated in the sequence presented in figures 8(a–d). In this sequence, the particles are represented by circles, and figures 8(a–d) correspond to times of flight of 7.2, 7.9, 8.6 and 9.4 ms, respectively. Figure 8(d) shows that almost all of the particles have completely vaporized by $3.25D$. Thus, these particles have little time to interact with the large vortices at the end of the transition region and are not dispersed beyond the jet mixing layer. Therefore, dispersion should be underpredicted by the type I approximation.

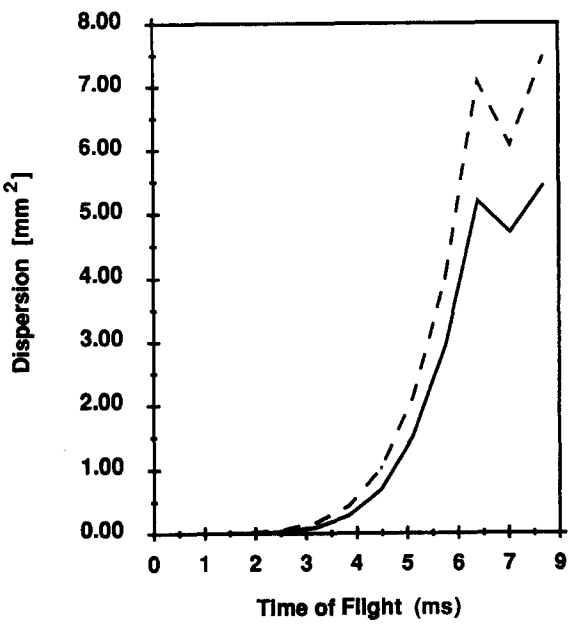

Figure 7. Radial disperions of varporizing, 150 μm octane particles in 1500 K air at 20 bar. – – –, General equation; ——, type I approximation.

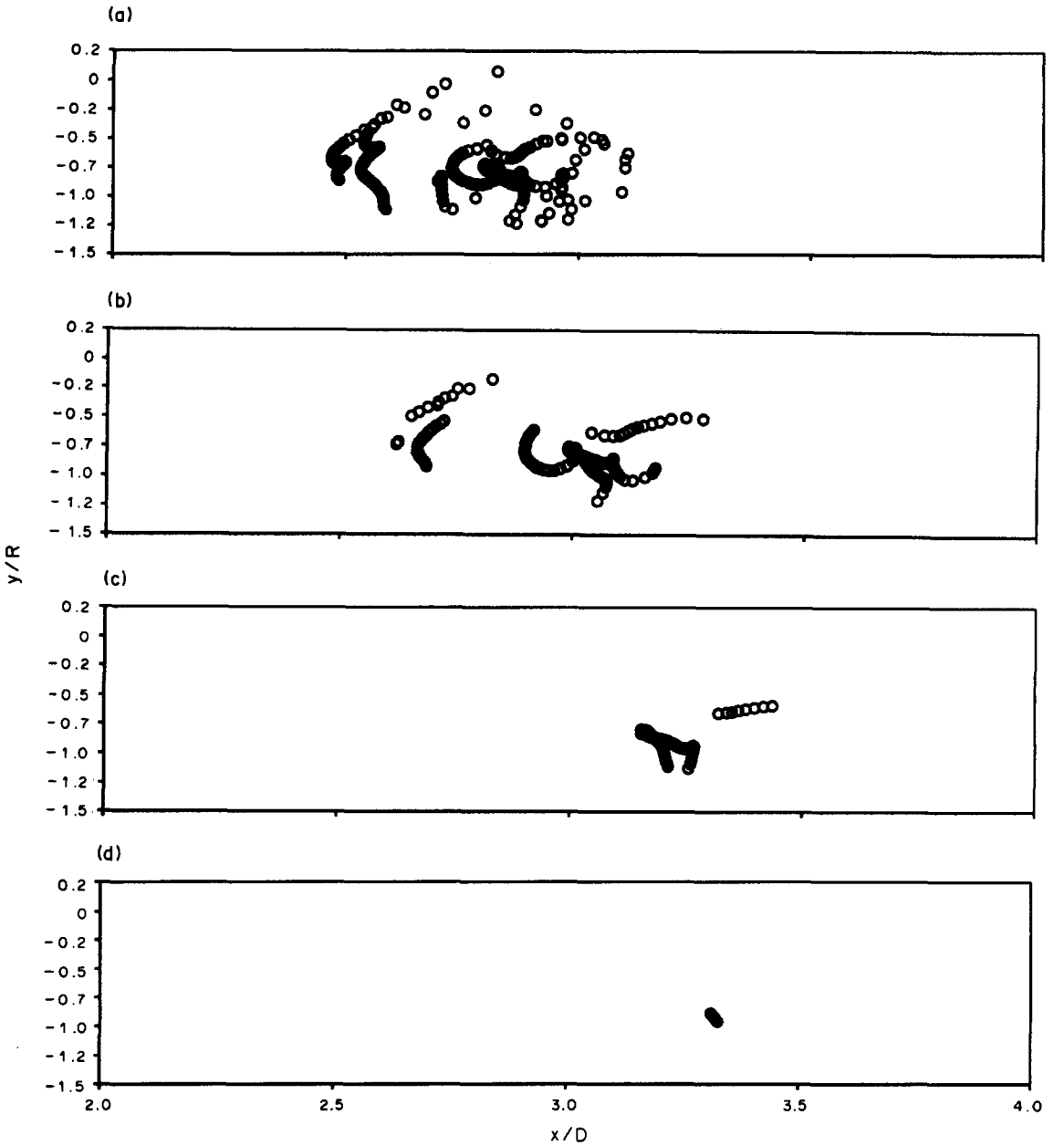

Figure 8. Particle positions for vaporizing, 150 μm octane particles in 1500 K air at 20 bar at times of flight of: (a) 0.0072 s; (b) 0.0079 s; (c) 0.0086 s; (d) 0.0094 s.

The relative difference between dispersion predicted by the type I approximation and that given by the general case is largest at early times of flight where the relative difference may be as great as 80% at times on the order of 1 ms. This difference is caused by the low value of drag and the high value of f_r in the near-nozzle region. The error in dispersion decreases from its peak value near the nozzle but it still remains large downstream, approaching a fairly constant value of about 25%. This indicates that it is advisable that the general equation is used for large particles vaporizing under typical combustor conditions in order to obtain reasonable estimates of particle dispersion. This conclusion, of course, presupposes the validity of the modified BBO equation under these conditions; this is still open to question. Nevertheless, given the use of this equation in spray models, a self-consistent treatment of the problem would suggest that turbulent dispersion under combustor conditions may require consideration of terms in addition to drag.

5. CONCLUSIONS

In this study it was found that circumferential velocity fluctuations do not play a major role in particle dispersion in the transition of a round jet. This is an important conclusion because it validates the use of axisymmetric models for the transition region, which may yield large reductions in computational time.

The Basset, virtual mass, fluid and buoyancy forces were found to increase in importance relative to the drag force as the particle diameter and the pressure increased for a fixed efflux of momentum and jet structure. At low pressures or for large ratios of particle to gas density, the Basset force was much more important than the fluid, virtual mass and buoyancy forces, while at high pressure all of the forces were of approximately equal significance, especially for large particles. Similar conclusions have been drawn in the past by Hjelmelt & Mockros (1966) and Lazaro & Lasheras (1989), but their conclusions were pertinent to Stokesian motion and were not developed for a turbulent shear flow. The results of this study show that these researchers' results are still relevant for non-Stokesian particle gas interactions and can provide reasonable, qualitative estimates of the situations when the complete set of forces should be included in a particle's force balance. The phenomenon of particles being "flung" outside the jet was described by Chung & Troutt (1988) and was confirmed in this study. At higher droplet Re values and pressures it was found that their nondimensional ratio of particle-to-gas time scales could not be used to predict this phenomenon reliably; a high Re correction to the particle response would be required.

This study has shown that by neglecting the Basset, virtual mass and fluid forces, radial dispersion will be underestimated while the particles are in the jet. Furthermore, for those particles which continue downstream after the last coalescence of rings, the Basset, fluid and virtual mass forces can still play a role in the dispersion process for large particles, even though the base flow frequency is reduced 8-fold. For instance, the error produced in radial dispersion by neglecting the Basset, virtual mass and fluid forces after the final coalescence was a constant 20% for the 150 μm dia particles in 1 bar, 300 K air.

The Basset, virtual mass and fluid forces were also found to be important for vaporizing, 150 μm, octane particles at a typical combustor pressure and temperature of 20 bar and 1500 K, respectively. In fact, the radial dispersion was underestimated by over 25% for a significant portion of the particles' history by using only the drag force. In order to correctly predict the behavior of a typical spray combustion system such as a gas-turbine combustor, consideration should be given to the inclusion of the Basset, virtual mass and fluid forces although computational penalties may prohibit an implementation of the full equation in a practical calculation.

Acknowledgement—This material is based upon work supported by the U.S. Air Force Office of Scientific Research under Award No. AFOSR-89-0392.

REFERENCES

ANDERSON, C. & GREENGARD, C. 1984 On vortex methods. *SIAM Jl Numer. Analysis* **22,** 413.

ASHURST, W. T. & MEIBURG, E. 1988 Three-dimensional shear layer via vortex dynamics. *J. Fluid Mech.* **189,** 87–116.

BASSET, A. B. 1888 *A Treatise on Hydrodynamics*, Vol. 2. Deighton-Bell, London.

BEATON, C. F. & HEWITT, G. F. 1989 *Physical Property Data of the Design Engineer*. Hemisphere, New York.

BOUSSINESQ, J. 1903 *Theorie Analytique de la Chaleur*, Vol. 2. Gauthier-Villars, Paris.

CHORIN, A. J. 1980 Vortex models and boundary layer instability. *SIAM Jl Sci. Statist. Comput.* **1,** 1.

CHORIN, A. J. 1990 Hairpin removal in vortex interactions. *J. Comput. Phys.* **91,** 1.

CHUNG, J. N. & TROUTT, T. R. 1988 Simulation of particle dispersion in an axisymmetric jet. *J. Fluid Mech.* **186,** 199–222.

CLIFT, R., GRACE, J. R. & WEBER, M. E. 1978 *Bubbles, Drop and Particles*. Academic Press, New York.

CROW, S. C. & CHAMPAGNE, F. H. 1971 Orderly structure in jet turbulence. *J. Fluid Mech.* **48,** 547–591.

FAETH, G. M. 1983 Evaporation and combustion of sprays. *Prog. Energy Combust. Sci.* **9,** 1–76.

HINZE, J. O. 1975 *Turbulence.* McGraw-Hill, New York.

HJELMFELT, A. T. & MOCKROS, L. F. 1966 Motion of discrete particles in a turbulent fluid. *Appl. Scient. Res.* **16,** 149–161.

KANURY, M. A. 1975 *Introduction to Combustion Phenomena.* Gordon & Breach, New York.

KARANFILIAN, S. K. & KOTAS, T. J. 1978 Drag on a sphere in unsteady motion in a liquid at rest. *J. Fluid Mech.* **87,** 85–96.

KUO, K. K. 1986 *Principles of Combustion.* Wiley, New York.

LAZARO, B. J. & LASHERAS, J. C. 1989 Particle dispersion in a turbulent, plane, free shear layer. *Phys. Fluids* **A1,** 1035–1044.

LEONARD, A. 1985 Computing three-dimensional incompressible flows with vortex elements. *A. Rev. Fluid Mech.* **17,** 523–559.

LUNDGREN, T. S. & ASHURST, W. T. 1989 Area-varying waves on curved vortex tubes with application to vortex breakdown. *J. Fluid Mech.* **200,** 283–307.

MAXEY, M. R. & RILEY, J. J. 1983 Equation of motion for a small rigid sphere in a non-uniform flow. *Phys. Fluids* **26,** 883.

MOORE, D. W. 1972 Finite amplitude waves on aircraft trailing vortices. *Aeronaut. Q.* **23,** 307–314.

OCKENDON, J. R. 1968. The unsteady motion of a small sphere in a viscous liquid. *J. Fluid Mech.* **34,** 229–239.

ODAR, F. 1966 Verification of the proposed equation for calculation of the forces on a sphere accelerating in a viscous fluid. *J. Fluid Mech.* **25,** 591–592.

ODAR, F. & HAMILTON, W. S. 1964 Forces on a sphere accelerating in a viscous fluid. *J. Fluid Mech.* **18,** 302–314.

OSEEN, C. W. 1927 *Hydrodynamik.* Akademische Verlagsgescellschaft, Leipzig.

PUTNAM, A. 1961 Integratable form of droplet drag coefficient. *ARS Jl* **31,** 1467–1468.

REID, R. C., PRAUSNITZ, J. M. & POLING, B. E. 1987 *The Properties of Gases and Liquids,* 4th edn. McGraw-Hill, New York.

RENKSIZBULUT, M. & YUEN, M. C. 1983 Experimental study of droplet evaporation in a high-temperature air stream. *J. Heat Transfer* **105,** 384–388.

RILEY, J. J. 1971 Ph.D. Thesis, The Johns Hopkins Univ., Baltimore, MD.

SHUEN, J. S., SOLOMON, A. S. P., ZHANG, Q. F. & FAETH, G. M. 1985 Structure of particle-laden jets: Measurements and predictions. *AIAA Jl* **23,** 396–404.

TCHEN, C. M. 1947 Mean value and correlation problems connected with the motion of small particles suspended in a turbulent fluid. Ph.D. Thesis, Delft, The Netherlands.

WHITE, F. M. 1984 *Heat Transfer.* Addison-Wesley, Reading, MA.

YUEN, M. C. & CHEN, L. W. 1976 On drag of evaporating liquid droplets. *Combust. Sci. Technol* **14,** 147–154.

YULE, A. J. 1978 Large-scale structure in the mixing layer of a round jet. *J. Fluid Mech.* **89,** 413–432.